Severe dual atmosphere effect at 600 °C for stainless steel 441

Patrik Alnegren*, Mohammad Sattari, Jan-Erik Svensson, Jan Froitzheim

Energy and Materials, Chalmers University of Technology, Kemivägen 10, 41296 Gothenburg, Sweden

HIGHLIGHTS

- We examine a low cost ferritic steel as material for SOFC interconnects.
- The study is aimed to investigate the dual atmosphere effect at low temperature.
- Severe breakaway corrosion was observed under dual-atmosphere but not in air only.
- SEM and TEM analysis of oxide scale cross-sections.

ARTICLE INFO

ABSTRACT

AISI 441 foils of 0.2 mm thickness were exposed in a dual atmosphere setup in which one side was exposed to air -3% H_2O and the other to Ar -5% $H_2 - 3\%$ H_2O. The experiment was performed at 600 °C and was referenced against exposures in air $+3\%$ H_2O on both sides. The exposure conditions were chosen to simulate the conditions of an interconnect in intermediate temperature solid oxide fuel cell stacks (IT-SOFC). A strong dual atmosphere effect was observed: local breakaway corrosion was discovered after only 1000 h on samples exposed to dual atmospheres. After 3000 h iron oxide had propagated to cover the entire surface area of the sample. In comparison, the samples exposed in single atmosphere formed thin protective chromia scales on both sides even after 3000 h of exposure.

© 2015 The Authors. Published by Elsevier B.V. This is an open access article under the CC BY-NC-ND license (http://creativecommons.org/licenses/by-nc-nd/4.0/).

1. Introduction

Solid oxide fuel cells (SOFC) distinguish themselves from other fuel cell technologies by their high efficiency and fuel flexibility and are commonly considered for stationary power generation and APU applications [1—3]. In stacks of solid oxide fuel cells individual cells, are separated by interconnects which provide the flow field pattern for the anode and cathode gases and electrical contact throughout the stack. Ferritic steels combine good machinability and mechanical properties with low cost compared to ceramic alternatives and are therefore the most common material choice for interconnects. Despite their low cost, metallic interconnects make up a considerable part of the total manufacturing cost of a stack [4]. Thus there are commercial incentives for finding low cost materials.

The corrosion stability of ferritic steels for interconnects rely on the formation of a passivating chromium oxide layer on the surface of the interconnect which limits the rate of oxidation by acting as a diffusion barrier. Long-term operation requires this chromia scale to grow slowly to maintain low electrical resistance over the interconnects [5,6]. Furthermore, the thickness of the oxide must be below a certain thickness to remain well adhered to the metal substrate and not spall off [7]. It is essential that chromium is preferentially oxidized over iron in the steel since iron oxides are much less protective and grow several orders of magnitude faster than chromium oxide. In order for a steel to form a continuous protective chromia scale, the supply, or flux, of chromium from the bulk alloy must be sufficiently high in comparison to the consumption of chromium at the oxide/metal interface by means of oxidation [8]. A common problem for SOFCs is that the high flow rate of ambient air on the cathode side causes evaporation of volatile chromium species which causes a reduction of the catalytic activity of the cathode [9,10]. Chromium evaporation also leads to increased chromium consumption from the steel interconnect. This reduces the predicted life time of the interconnect since the steel

* Corresponding author.
 E-mail address: patrik.alnegren@chalmers.se (P. Alnegren).

will be depleted of chromium faster which will cause the formation of iron oxide and consequently rapid oxidation, commonly referred to as breakaway oxidation [11,12].

Additionally, a special environmental situation found in fuel cells that can lead to increased degradation rate is the dual atmospheres of air on one side of the interconnect and fuel on the other. Several studies have shown that when simultaneously exposed to air and hydrogen on either side, ferritic steels tend to form iron rich oxide scales on the air side, which consequently leads to faster oxidation rates [13–16]. However, some authors have also reported similar oxidation behavior in dual conditions as when exposed separately in air or humid hydrogen atmosphere [17,18] which indicates that several other experimental conditions need to be taken into consideration. Most of these studies were carried out at temperatures of 800–900 °C. However, the development of SOFCs strives towards lower operating temperatures in order to decrease the degradation rate of cell components. Due to recent advances in SOFC technology an operating temperature of around 600 °C can be sufficient to maintain good ionic conductivity of the electrolyte [19]. Even though the oxidation rate of metals is expected to decrease at lower temperatures, several studies of FeCr alloys have shown that, depending on the exposure atmosphere and alloy composition, the oxidation rate can be increased when the temperature is decreased to certain temperature intervals [20–23]. This is likely caused by slower chromium diffusion towards the metal/oxide interface relative to the consumption of chromium from oxidation, which prevents the formation of a continuous chromia scale. Young et al. have studied several ferritic steels in a simulated anode side SOFC atmosphere at temperatures ranging from 500 to 900 °C [22]. They found that oxidation was generally more severe in the 500–650 °C region than in the 650–800 °C region because more iron oxide nodules were formed at lower temperatures.

A number of environment parameters must be taken into account when designing interconnect materials for SOFC applications. The current study is intended to investigate the feasibility of using ferritic steels at lower operating temperature. The aim of this study is to investigate the long term effects of dual atmosphere exposure at 600 °C for a ferritic steel considered for application as interconnect material. AISI 441 was chosen as the test material because it is a low cost alternative compared to commercial SOFC grade alloys, e.g. Crofer 22 APU, Crofer 22H, Sanergy HT or ZMG 232. Test conditions were chosen to replicate the conditions within a fuel cell. Thus a setup with a high air flow rate was used to increase chromium evaporation.

2. Experimental

In order to simulate the conditions in a SOFC stack AISI 441 steel samples were simultaneously exposed to air -3% H_2O on one side and Ar -5% $H_2 - 3\%$ H_2O on the other at 600 °C. The dual atmosphere condition was achieved by placing circular steel samples in a sample holder based on a design from the National Energy Technology Laboratory (see Fig. 1). The dimensions for such a sample holder were provided by Montana State University and more information about the setup can be found in [15,24,25]. The sample holder used in this study was produced from 253 MA steel with adaptors welded to 6 mm 316 L steel tubes. Gold gaskets were used to seal the steel samples to the sample holder, and gas tightness was controlled before, during and after exposure. The sample holder was placed in a 60 mm diameter silica tube in a tubular furnace.

One side of the sample holder was used for reference testing, in order to differentiate possible dual atmosphere effects, and was fed with humid air on both sides. Thus, two samples were exposed to

dual conditions and the other two samples were exposed to single conditions of air on both sides. The flow rates were 400 sml min^{-1} air $-$ 3% H_2O for the air side inside the sample holder, 100 sml min^{-1} Ar -5% $H_2 - 3\%$ H_2O for the hydrogen side inside the sample holder and 8800 sml min^{-1} air $-$ 3% H_2O outside the sample holder. An absolute humidity level of 3% was achieved for all gas streams by leading the gases through Nafion membranes (Perma-Pure) which were fed with 24.4 °C deionized water. The humidity level was checked using a chilled mirror humidity sensor (Michelle − Optidew Vision). The flow rates for the air were chosen to achieve an average flow speed of approximately 27 cm s^{-1} and were calculated from the dimension of the inside and outside (silica tube diameter) of the sample holder. Based on a previous study, this rate should be in a flow regime in which the chromium evaporation rate is kinetically controlled, i.e. independent of flow rate [26]. After 1000 h of exposure the furnace was cooled to room temperature and one set of samples was removed for analysis and the exposure was then continued up to 3000 h. In addition, a heating/cooling rate of 5 °C min^{-1} was used and the setup was flushed for at least 12 h before heating was initiated.

AISI 441 steel with a 0.2 mm thickness was cut into 20 mm diameter circular samples. Compositional information of the steel is given in Table 1. The samples were cleaned in ultrasonic bath in acetone and ethanol. All samples, in the as-received state (no polishing), were pre-oxidized for 3 h in ambient air at 800 °C to mimic the sintering step in SOFC stack production. Pre-oxidation led to mass gains of 0.022 mg cm^{-2} on average, which should correspond to an oxide scale thickness of 140 nm if the oxide is assumed to be dense chromia. The samples were photographed after exposure, and a detailed analysis was performed with electron microscopy. A Zeiss LEO ULTRA 55 FE-SEM scanning electron microscope (SEM) equipped with an Oxford Instruments INCA X-Sight energy-dispersive X-ray spectroscopy (EDX) system was used, as well as an FEI Titan 80−300 scanning transmission electron microscope (STEM). Samples for TEM were prepared by focused ion beam (FIB) milling and in-situ lift-out technique in an FEI Versa 3D DualBeam instrument. A Leica EM TIC 3X broad ion beam (BIB) instrument was used in order to prepare wide cross sections (in the range of mm) of the samples.

3. Results

3.1. Visual inspection

In Fig. 2, photographs of the air sides (outer side of sample holder) of all the exposed samples after 1000 h and 3000 h are displayed. After 1000 h, both samples exposed to the dual atmosphere conditions had areas of thick, grey-colored thicker oxides which covered around 20% of the sample surface area. The rest of the sample area exhibited a shiny metallic surface which indicates a thin oxide. In contrast, the samples exposed to single atmosphere had a shiny surface all over the sample area except for some small spots of darker-colored oxide. A comparison of photographs of the single-atmosphere-exposed samples after 1000 h and 3000 h shows that the oxide spots did not seem to grow considerably after 1000 h. By comparison, the thick, grey colored oxide had propagated to almost cover the entire surface area for of dual-atmosphere-exposed sample after 3000 h. The hydrogen sides of the samples exposed to the dual atmosphere displayed shiny surfaces, similar to those found on the samples exposed to the single atmosphere, except some minor thicker oxide nodules on the 3000 h samples. More detailed analyses of the oxide scales grown on the samples will be presented below.
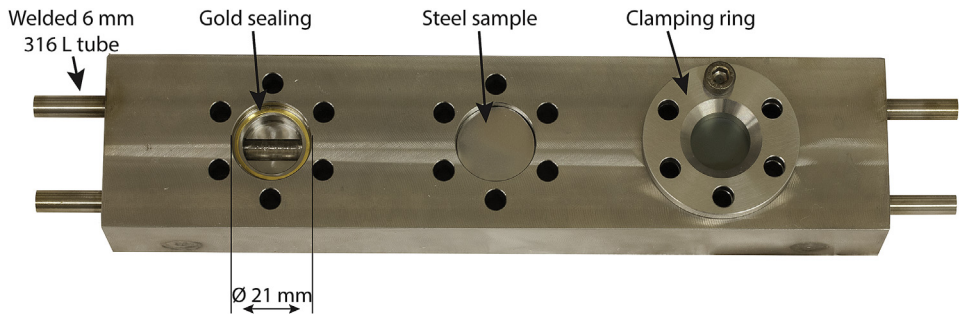
Fig. 1. Sample holder for the dual atmosphere setup. Each step in the mounting sequence of samples is demonstratively shown from left to right.

Table 1
Composition of the investigated steel batch in weight %. The composition was given by Sandvik Materials Technology who provided the steel.

Material	Fe	Cr	Mn	Si	Ti	Nb	C	S
AISI 441	Bal	17.7	0.30	0.55	0.15	0.37	0.015	0.002

3.2. Analysis after 1000 h

Fig. 3(a and b) show micrographs of the microstructure of the sample exposed to the single atmosphere. Most of the surface exhibited a thin and protective oxide consisting of a thin base oxide and evenly distributed cubic crystal nodules up to 1 μm in size. The cubic oxide grains were rich in manganese and chromium. The crystal phases could not be identified using XRD due to bending of the samples after removal from the sample holder after exposure, but can be assumed to consist of two oxide phases where the cubic nodules are assumed to be spinel phase $(Cr,Mn)_3O_4$ and the thin base oxide is expected to be a corundum structure Cr_2O_3 oxide, as reported by other authors for manganese-containing ferritic steels after exposure in air at 650 °C [27]. A few iron-rich oxide islands in the 100 μm range with whisker type morphology were found in some areas of the sample exposed to the single atmosphere.

In Fig. 3(c and d) the morphology of the oxide scale, including EDX elemental maps, of the air side of a sample exposed for 1000 h to the dual atmosphere is displayed. Two types of oxide morphologies were found on the sample: Approximately 20% of the surface was covered with a thicker oxide with whisker type morphology that appears darker in the backscattered images since less signal is received from the alloy beneath the oxide than from the thinner parts. The rest of the surface was covered by a thinner oxide with similar morphology as the oxide formed on the sample exposed to the single atmosphere, with cubic manganese-rich grains on a chromium oxide surface. Fig. 4 shows broad ion beam (BIB) cross sections of the thin parts of the oxide on both the single-atmosphere and dual-atmosphere exposed samples. By comparison of the yet protective parts on the air side of the dual-atmosphere-exposed sample, with the hydrogen side and the sample exposed to the single atmosphere, it seems that both the morphology and oxide thickness are very similar. EDX elemental analysis (see Fig. 3d) revealed that the thicker oxide parts formed on the air side of the dual-atmosphere-exposed sample exclusively consisted of iron oxide (96% cation Fe measured by EDX). The protruding nature of the whisker type morphology of the iron oxides indicates outward growth [28]. Furthermore, the iron oxides are expected to adopt the hematite structure in atmospheres of air [8], which has also been reported by others in dual atmosphere conditions at 800 °C [13,15,25].

In order to obtain information about the propagation and initiation of the thick iron oxide on the air side of the dual-atmosphere exposed sample, a cross section lamella of a small oxide island formed on the air side of a dual atmosphere sample, exposed for 1000 h, was prepared for TEM investigation. Fig. 5 contains STEM images of the cross section and elemental information from EDX. The oxide nodule was found to consist of three
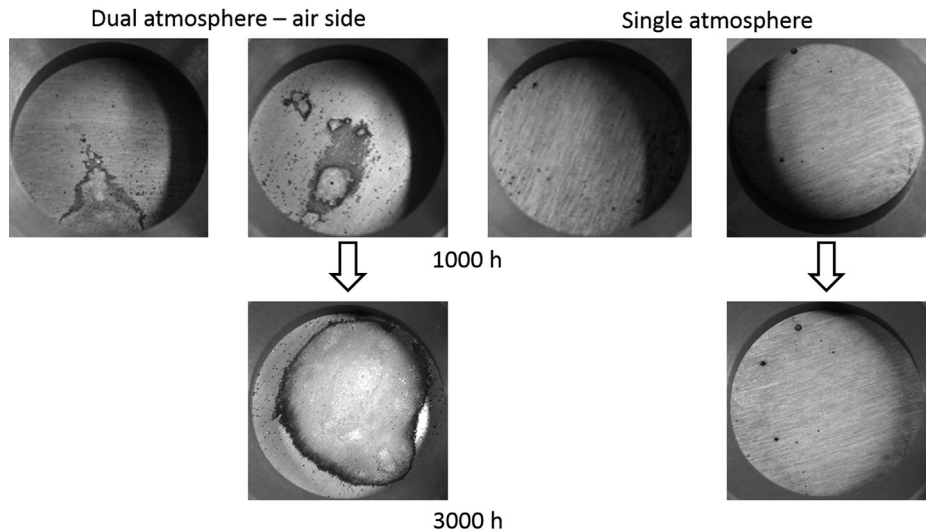

Fig. 2. Photographs of the exposed samples after 1000 h and 3000 h. The arrows indicate the samples which were left for exposure up to 3000 h.

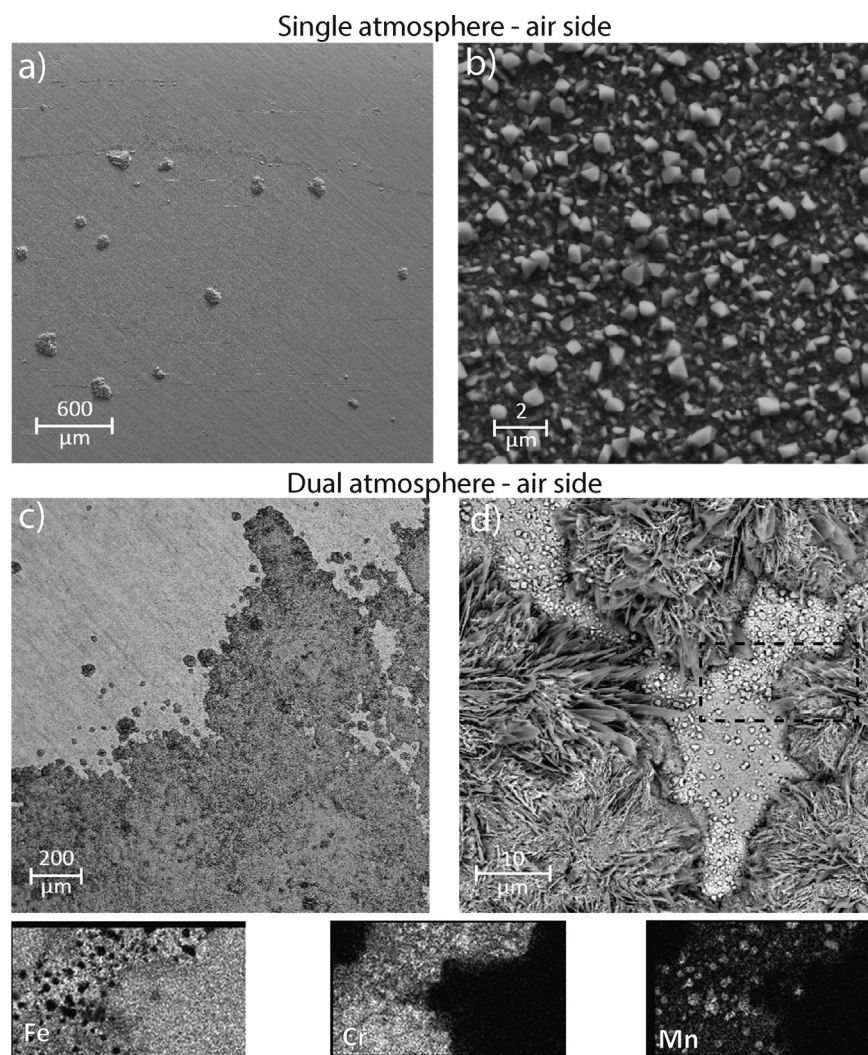Single atmosphere - air side

Dual atmosphere - air side

Fig. 3. Micrographs of the surface of samples exposed for 1000 h. a) and b) show a sample exposed to the single atmosphere, different magnifications. c) and d) show the air side of a sample exposed to dual atmosphere conditions, different magnifications. The dashed line box in d) shows where the elemental EDX maps (which are plotted below) were retrieved.

main regions: i) an iron-rich outer oxide (~95% Fe cation measured with EDX), presumably hematite, ii) an inwards progressing iron-chromium (50—60% Cr cations) oxide with a porous structure and iii) an inner part of iron-chromium oxide mixed with not yet oxidized metal. Additionally, a chromium oxide layer can be seen in Fig. 5, stretching from the protective thin oxide side through the iron oxide nodule. The inner iron-chromium oxide zone propagated within one grain of the alloy, and stopped at the grain boundary, which was enriched in chromium oxide. In addition, a silica sub-layer was found underneath the chromia scale, and internal pre-cipitates of titanium oxide were also found (not shown here).

3.3. Analysis after 3000 h

After 3000 h exposure, the sample exposed to the single at-mosphere (see Fig. 6(a and b)) had an oxide surface very similar to the sample exposed for 1000 h and almost the entire surface was covered by a thin oxide scale. Some nodules of iron oxide were found but these were not significantly larger than those found after 1000 h exposure. In Fig. 6(c and d), a plan view image of the transition region between protective and non-protective oxide on the air side of a dual-atmosphere-exposed sample is shown. This

transition region had morphology very similar to the sample exposed for 1000 h, but after 3000 h, most of the sample surface was covered with whisker-type iron oxide. The hydrogen side of the same sample (see Fig. 6(e and f)) mostly resembled that of the sample exposed to the single atmosphere, with cubic crystals on a dense chromium oxide layer. However, some larger oxide nodules with cubic grains of iron oxide were also discovered. In Fig. 7, a BIB cross section, including elemental maps, of the oxide formed on the air side of the dual-atmosphere-exposed sample is shown. An evenly thick double-layer oxide scale of approximately 40 μm was seen over the entire cross section. The composition resembles that of the non-protective oxide grown after 1000 h (Fig. 5) with an iron oxide outer phase and an inner iron-chromium oxide. The former grains of the alloy are visible in the inner oxide region, with what looks to be an enrichment of chromium in around along the grain boundaries. After 3000 h the chromia layer from the initial pre-oxidation step could not be seen as clearly at the inward/outward oxide interface as after 1000 h of exposure.

4. Discussion

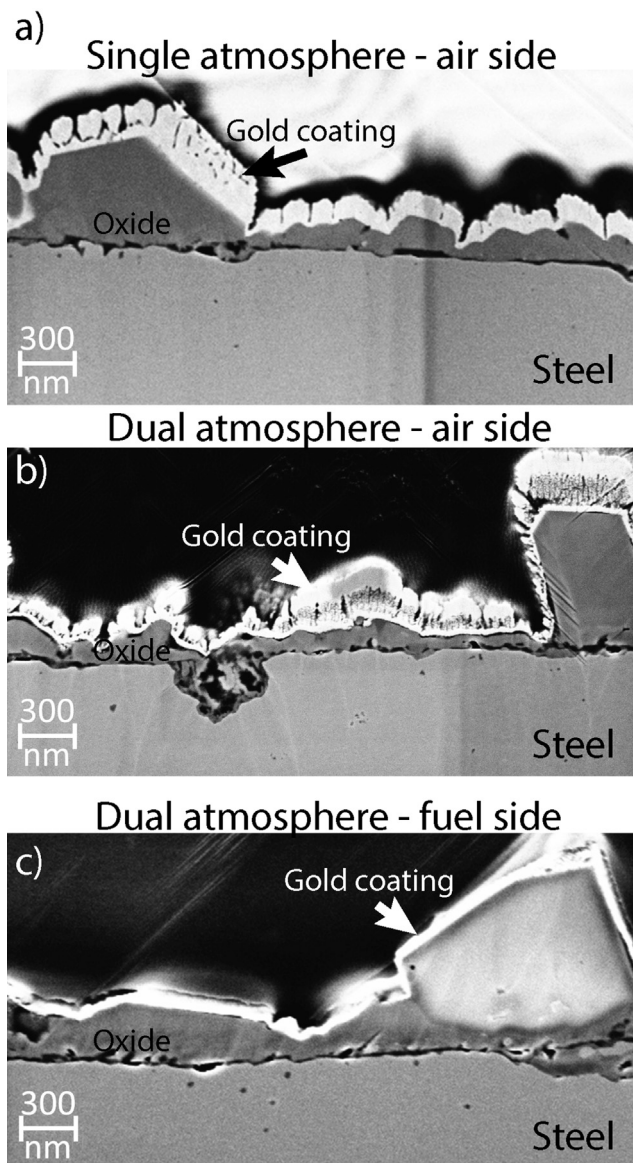In this study, a dramatic change in degradation rate was noticed

Fig. 4. Micrographs of protective parts of the oxide on samples exposed for 1000 h. a) shows a sample exposed to the single atmosphere. b) shows the air side of a sample exposed to the dual atmosphere and c) the hydrogen side of the same sample.

when a ferritic steel was exposed to a dual atmosphere of humid hydrogen on one side and air on the other, like it would be inside a SOFC stack, in contrast to being exposed to a single atmosphere of humid air on both sides. The pre-oxidation step simulates the process of stack manufacturing but is also expected to provide a protective chromia scale that acts as a diffusion barrier both against the oxidation of the alloy and the transport of hydrogen from the hydrogen side to the air side [13]. Kurokawa et al. carried out hydrogen permeation measurements at 800 °C on Fe–16Cr steel and found that once a continuous Cr_2O_3 scale is formed the hydrogen permeation is drastically reduced because the permeability of hydrogen through Cr2O3 is approximately four orders of magnitude lower compared to the steel. This is in line with a study by Amendola et al. (at 800 °C) observing that a pre-oxidation for 100 h in air of Crofer 22 APU samples suppresses the dual-atmosphere effect [29]. However in the present study it is obvious that the pre-oxidation was not sufficient to suppress a dual atmosphere effect. Apart from the difference in temperature (600

vs. 800 °C) this can be attributed to the shorter pre-oxidation time (2 vs. 100 h). It is suggested that initially a protective chromia layer is formed but at some point, the chromia layer lost its protective behavior at some locations, and iron oxides were formed. The growth rate of iron oxide is much faster than chromia resulting in rapid oxide growth (breakaway corrosion). These breakaway areas propagated laterally to cover most of the sample surface after 3000 h of exposure. Such rapid degradation is of course detrimental for an interconnect material due to increased electrical losses and imminent mechanical failure of the steel. This rapid degradation will be discussed more in detail below.

4.1. Propagation of iron oxide

The initiation of the breakaway oxidation, on the air side of the dual-atmosphere-exposed sample, occurs not evenly over the entire sample surface. Instead it appears that the breakdown of the oxide scale starts in one or few spots and then propagates laterally (see Fig. 2). Fig. 5 depicts a TEM image of a cross-section through one of a newly formed oxide islands. The oxidation occurred through an outward growth of almost pure hematite and an inward growth of iron-chromium oxide. This inner oxide is expected to be a spinel phase of $(Fe,Cr)_3O_4$ based on EDX measurements and literature data by Liu et al. on the breakaway oxidation of a ferritic steel oxidized at 600 °C [30]. The porous structure of the inner oxide is formed as a result of the outward diffusion of iron, which leaves voids within the oxide [31]. The most inner parts of this region consisted of metal mixed with oxide, a phenomenon reported by others as well, e.g. [22,31,32]. This has been suggested by Puji-laksono et al. to occur due to an immiscibility gap in the Fe–Cr–O spinel phase system, resulting in this metal/oxide mix [32]. The propagation of this inward-growing oxide seemed to have stopped at the grain boundary of the alloy based on the observation after 1000 h of exposure (see Fig. 5). This is likely due to the faster chromium diffusion within alloy grain boundaries, which consequently leads to formation of a more protective chromium-rich oxide which is supported by the EDX analysis in Fig. 5, where the grain boundary to the left of the inward growing oxide indeed shows a chromium enrichment in the EDX map. Remnants of the initially formed chromia layer, at the interface between the inward and outward growing oxides, are still clearly visible after 1000 h of exposure but less visible after 3000 h (see Fig. 7). After 3000 h, an enrichment of chromium is visible at the former alloy grain boundaries for the inner oxide layer which makes it unlikely that the inner oxide propagates through the grain boundaries. Based on these observations it is suggested that hematite grows outwards, spreads laterally and dissolves the initial chromia layer. Thus the chromia scale becomes more iron rich and less protective which leads to the initiation of an inward/outward breakaway oxidation at the next alloy grain. Support for such a mechanism can be seen in Fig. 8, where initiation of an inward growing oxide was seen to occur within an alloy grain and not in contact with the inward oxide from the grain next to it. This behavior also explains the observed non-uniform oxidation behavior, with an initiation site followed by lateral growth.

Some iron-rich oxide was found also on the hydrogen side after 3000 h of the dual atmosphere exposed sample. However, since only few such iron-rich nodules were found, this could also be due to sample defects present before exposure. From a technical perspective, this minor iron oxide formation is of less relevance since the severe corrosion on the air side should at this point have already caused major degradation in the performance of a SOFC stack and the nodules were therefore not investigated in detail.
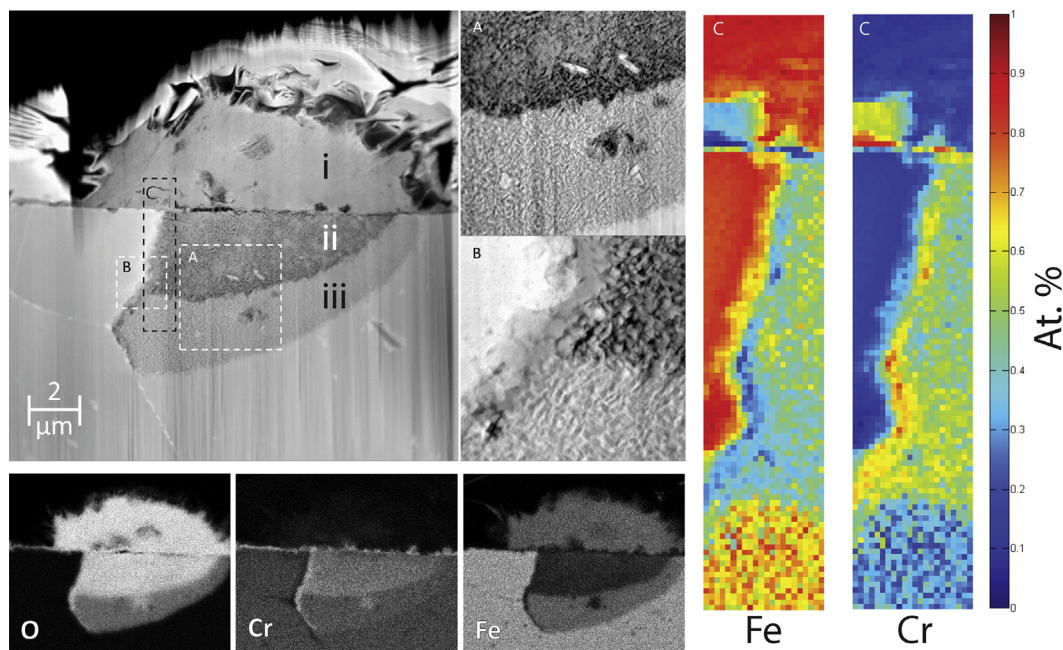
Fig. 5. TEM image of an iron oxide nodule grown on the air side of a dual atmosphere sample exposed for 1000 h, including elemental EDX maps from SEM (below) and from STEM (to the right). i) outward growing Fe_2O_3, ii) inward growing $(Fe,Cr)_3O_4$, iii) reaction zone with mixed oxide and unreacted metal.

4.2. Dual atmosphere effect

For a chromia layer to be protective it must be continuous and cover the entire alloy surface. Thus, chromium needs to be preferentially oxidized over iron. Despite its higher affinity for oxygen, chromium needs to have sufficient activity for a continuous scale to form. Furthermore, in order for the chromia scale to stay protective the supply of chromium from the alloy must be faster than the consumption of chromium at the metal/oxide scale-interface in order to maintain a critical concentration of chromium [22,33,34]. Evaporation of volatile chromium species increases the rate of chromium consumption from the oxide scale and can cause breakaway corrosion, which has been shown both for austenitic and ferritic steels [12,30]. In addition, Young et al. have shown that in atmospheres of 4% H_2/20% H_2O (i.e. simulated SOFC anode environment) the critical concentration of chromium required for maintaining a protective chromia scale increases with lower temperatures and at 600 °C iron oxide formation was seen for several different steels [22]. Those authors explained this inverse temperature effect by a higher activation energy for chromium diffusion in the alloy than for oxidation of chromium in humid hydrogen atmospheres. However, with the same model, using values from Fe20Cr steels in 20% O_2, those authors also predicted that in such an environment the critical chromium concentration would decrease with decreasing temperature.

The most severe corrosion in the present study occurred on the air side of the dual-atmosphere-exposed sample. This environment resembles the 20% O_2 atmosphere used for predicting the temperature dependence of critical chromium concentration by Young et al. [22]. Using their model, the severe breakaway corrosion seen in this study should not occur due to the low exposure temperature of 600 °C. However, according to measurements of Fe22Cr steels at 650 °C by Falk-Windisch et al. [27], the major chromium consumption, at the high flow rates and 3% humidity used in this study, should be due to chromium evaporation. Falk-Windisch et al. reported an activation energy of 91 kJ mol^{-1} for chromium evaporation, which can be compared to a calculated activation energy for

chromium diffusion in chromium steels of 179 kJ mol^{-1} by Young et al. [22], using data from chromium depletion profiles obtained at 900–1200 °C by Whittle et al. [35], which would explain the more severe formation of iron oxides in this study compared to other studies performed at higher temperatures [13–18]. Thus, higher chromium contents in the alloy should be required at lower temperature if there is considerable chromium evaporation. Nevertheless, chromium evaporation alone was not enough to cause breakaway corrosion, as seen here for the samples exposed to the single atmosphere. Apparently, hydrogen present on the reverse side of the sample affects either the supply or the consumption of chromium.

It has been shown that hydrogen can diffuse relatively fast through a steel sheet and at 600 °C a permeation rate in the order of mm h^{-1} can be expected [36] and SIMS measurements confirmed higher hydrogen concentration in the steel under dual atmosphere conditions [16]. Nevertheless, the exact mechanism on how permeated hydrogen affects the air side oxide properties is unknown. Rufner et al. suggested that permeated hydrogen locally alters the pO_2 on the air side, however it is not obvious how this promotes the formation of Fe-rich oxides. Yang et al. suggested that hydrogen is incorporated into the air side oxide scale as hydroxide ions, where these defects are compensated by extra metal vacancies which increases the outward diffusion of metal ions [13]. If this were the case, the oxides formed on the air side of a dual-atmosphere-exposed sample before breakaway would be expected to grow thicker than the oxides formed on the samples exposed to the single atmosphere. In Fig. 4, cross sections of protective oxides formed after 1000 h in dual and single atmospheres are depicted. From these micrographs it was not possible to distinguish any difference in oxide thickness, but minor differences would be difficult to differentiate since the scales vary in thickness along the sample surface. Hydrogen has also been suggested, by Essuman et al. to cause increased oxygen inward diffusion due to increased oxygen solubility in the alloy and/or increased diffusion rate due to lattice distortion caused by hydrogen in the alloy [37,38]. Those authors suggested that this leads to internal
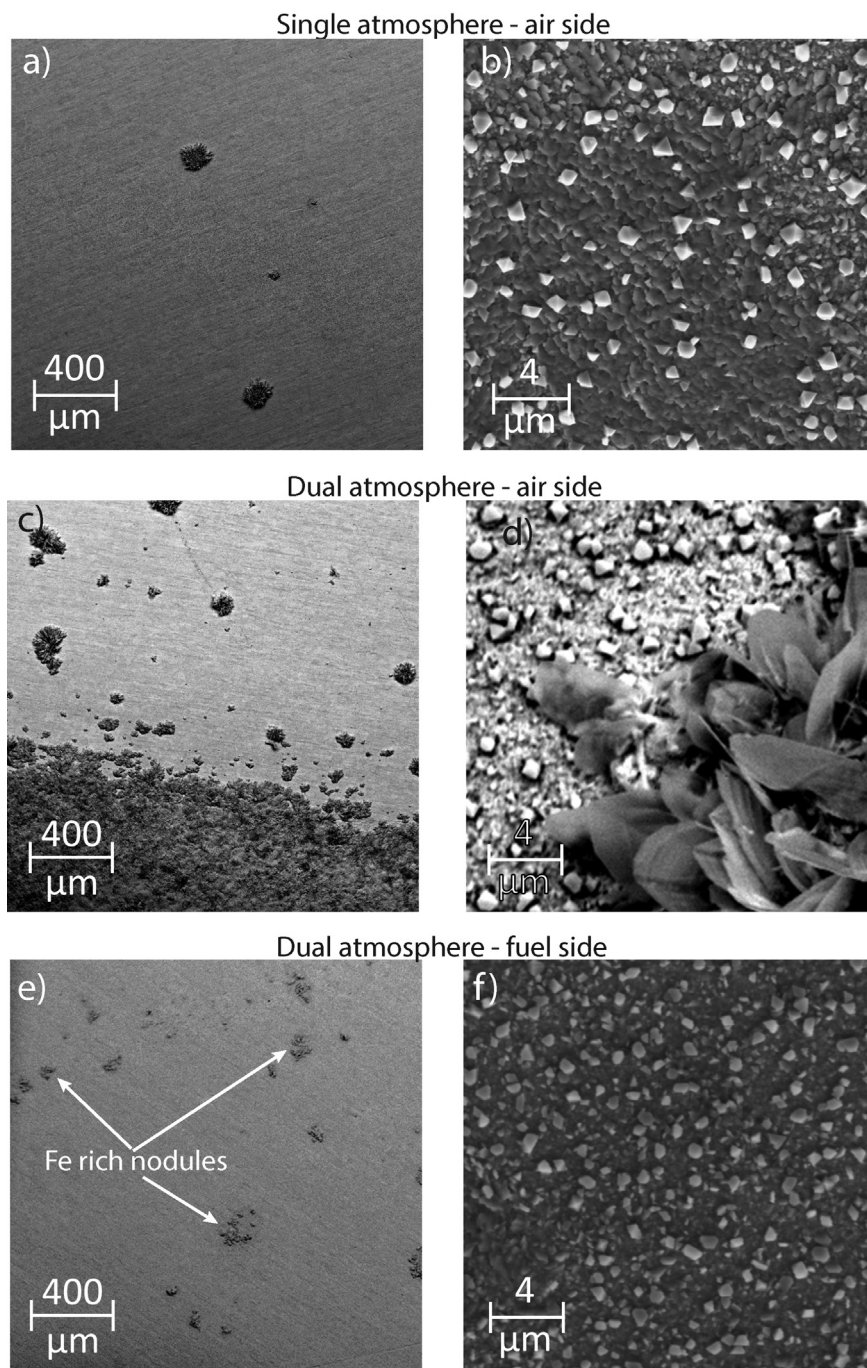
Single atmosphere - air side

Dual atmosphere - air side

Dual atmosphere - fuel side

Fig. 6. Micrographs of the surface of samples exposed for 3000 h. a) and b) show a sample exposed to the single atmosphere, different magnifications. c) and d) show the air side of a sample exposed to the dual atmosphere, different magnifications and e) and f) the hydrogen side of the same sample. f) shows an area without any iron rich oxide nodules.

oxidation which reduces the supply of chromium and causes breakaway oxidation. For the sample exposed to a dual atmosphere, local spots of inward growing oxide were noted beneath a thin chromia scale as can be seen in Fig. 4. These could be initiation points for breakaway corrosion. However, more detailed studies are needed to confirm such a mechanism.

The extent of corrosion observed in this study is much more severe than what has been reported by others in dual conditions [13—18]. It seems that the combined environment of reduced exposure temperature, high flow rate with humid air and the presence of hydrogen on the other side of the substrate is

challenging for the Fe18Cr ferritic steel AISI 441 and long operating times for a SOFC cannot be expected if this steel is used as interconnect material. It was seen here that pre-oxidation for 3 h at 800 °C was not sufficient to provide good protection against a dual atmosphere. Ferritic steels with higher chromium contents are expected withstand this effect for a longer time period [13,22,23]. However, at a lower operating temperature, increasing the chromium content increases the risk of sigma phase formation within the alloy which leads to embrittlement of the interconnect [39—41]. Niewolak et al. investigated different ferritic and austenitic steels at 600 °C in air and simulated fuel environment (humidified
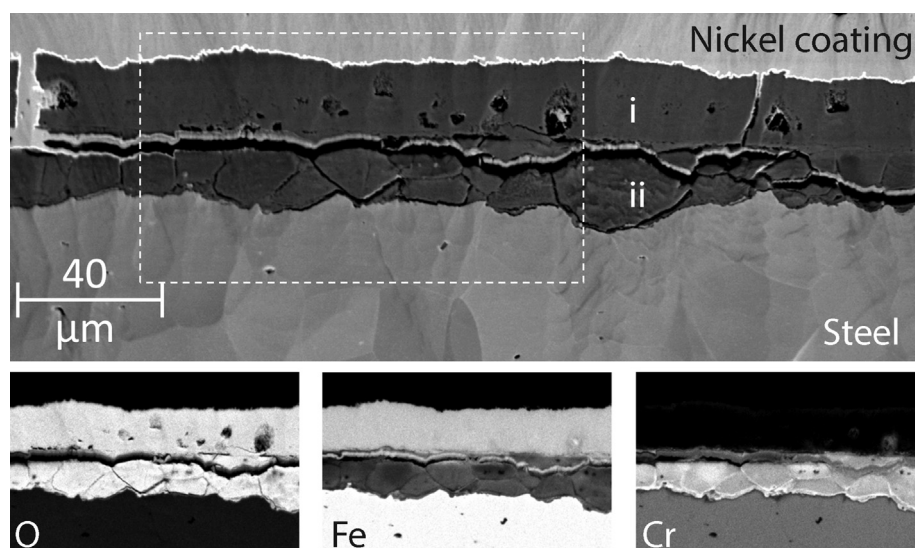
Fig. 7. Micrograph of a cross-section and elemental EDX maps on the air side of a sample exposed to the dual atmosphere for 3000 h. i) outward growing Fe_2O_3, ii) inward growing $(Fe,Cr)_3O_4$.
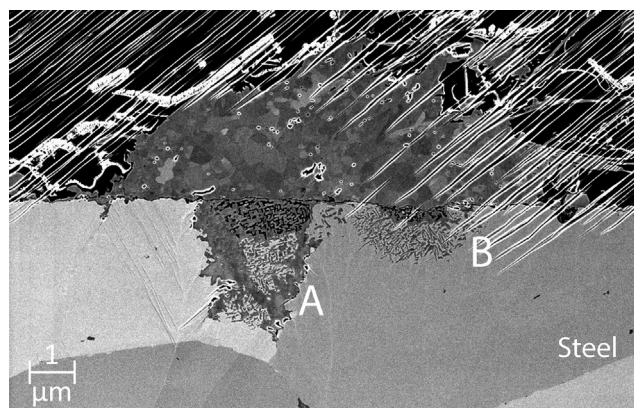

Fig. 8. Micrograph of a cross-section of an iron oxide nodule formed on the air side of a sample exposed to the dual atmosphere for 1000 h. A: suggested first spot of breakaway oxidation, B: suggested second site for breakaway oxidation.

hydrogen) and found that steels with low chromium content were prone to form non-protective iron oxide scales in fuel environment [42], but also found that when the steels were #1200 grit grounded the ability to form a protective chromia scale greatly improved, which is attributed to higher concentration of diffusion paths which increases chromium re-supply. Other possible solutions could include longer pre-oxidation times or coatings to protect against chromium evaporation [5,26,43], decrease corrosion rate [44–46] or dedicated coatings to decreases hydrogen diffusion.

5. Conclusions

When exposed to dual atmosphere conditions with humid hydrogen on one side and humid high flow air on the other side, the ferritic steel AISI 441 went into breakaway corrosion after 1000 h of exposure. The formed iron oxides consisted of an outward growing hematite phase and an inward growing iron-chromium oxide. No sign of breakaway oxidation was seen for reference samples exposed to humid air on both sides, thus it was concluded that hydrogen present on one side of the sample affects the oxidation mechanism of the air side. This dual atmosphere effect was possibly accelerated by a combined effect of the low exposure temperature of 600 °C and by chromium loss due to volatilization of chromium species due to a high flow rate of humid air. The hydrogen must diffuse through the steel substrate and either decreases the supply of chromium from the bulk alloy or affect the rate of oxidation, but more studies are necessary in order to conclude the exact mechanism of this dual-atmosphere effect. The current exposure conditions should represent conditions found within an operating IT-SOFC stack, and thus the use of uncoated AISI 441 as interconnect material seems unsuitable for long-term operation.

References

[1] F. Baratto, U.M. Diwekar, Life cycle assessment of fuel cell-based APUs, J. Power Sources 139 (2005) 188–196, http://dx.doi.org/10.1016/j.jpowsour.2004.07.025.

[2] N. Minh, Solid oxide fuel cell technology – features and applications, Solid State Ionics 174 (2004) 271–277, http://dx.doi.org/10.1016/j.ssi.2004.07.042.

[3] I. Staffell, A. Ingram, K. Kendall, Energy and carbon payback times for solid oxide fuel cell based domestic CHP, Int. J. Hydrogen Energy 37 (2012) 2509–2523, http://dx.doi.org/10.1016/j.ijhydene.2011.10.060.

[4] T.D. Hall, H. McCrabb, J. Wu, H. Zhang, X. Liu, J. Taylor, Electrodeposition of CoMn onto stainless steels interconnects for increased lifetimes in SOFCs, in: Solid Oxide Fuel Cells 12 (SOFC XII), Electrochemical Society Inc, 65 S Main St, Pennington, NJ 08534-2839 USA, 2011, pp. 2489–2502, http://dx.doi.org/10.1149/1.3570247.

[5] J.G. Grolig, J. Froitzheim, J.-E. Svensson, Coated stainless steel 441 as interconnect material for solid oxide fuel cells: oxidation performance and chromium evaporation, J. Power Sources 248 (2014) 1007–1013, http://dx.doi.org/10.1016/j.jpowsour.2013.08.089.

[6] K. Huang, Characterization of iron-based alloy interconnects for reduced temperature solid oxide fuel cells, Solid State Ionics 129 (2000) 237–250, http://dx.doi.org/10.1016/S0167-2738(99)00329-X.

[7] W.N. Liu, X. Sun, E. Stephens, M.A. Khaleel, Life prediction of coated and uncoated metallic interconnect for solid oxide fuel cell applications, J. Power Sources 189 (2009) 1044–1050, http://dx.doi.org/10.1016/j.jpowsour.2008.12.143.

[8] P. Kofstad, High Temperature Corrosion, Elsevier Applied Science Publishers Ltd., New York, 1988.

[9] S.P. Jiang, X. Chen, Chromium deposition and poisoning of cathodes of solid

oxide fuel cells − a review, Int. J. Hydrogen Energy 39 (2014) 505−531, http://dx.doi.org/10.1016/j.ijhydene.2013.10.042.

[10] C. Key, J. Eziashi, J. Froitzheim, R. Amendola, R. Smith, P. Gannon, Methods to quantify reactive chromium vaporization from solid oxide fuel cell interconnects, J. Electrochem. Soc. 161 (2014) C373−C381, http://dx.doi.org/10.1149/2.0041409jes.

[11] R. Sachitanand, J.-E. Svensson, J. Froitzheim, The influence of Cr evaporation on long term Cr depletion rates in ferritic stainless steels, Oxid. Met. (2015), http://dx.doi.org/10.1007/s11085-015-9552-5.

[12] H. Asteman, J.-E. Svensson, M. Norell, L.-G. Johansson, Influence of water vapor and flow rate on the high-temperature oxidation of 304L; effect of chromium oxide hydroxide evaporation, Oxid. Met. 54 (2000) 11−26, http://dx.doi.org/10.1023/A:1004642310974 (n.d.).

[13] Z. Yang, M.S. Walker, P. Singh, J.W. Stevenson, T. Norby, Oxidation behavior of ferritic stainless steels under SOFC interconnect exposure conditions, J. Electrochem. Soc. 151 (2004) B669, http://dx.doi.org/10.1149/1.1810393.

[14] Z. Yang, G. Xia, P. Singh, J.W. Stevenson, Effects of water vapor on oxidation behavior of ferritic stainless steels under solid oxide fuel cell interconnect exposure conditions, Solid State Ionics 176 (2005) 1495−1503, http://dx.doi.org/10.1016/j.ssi.2005.03.019.

[15] J. Rufner, Oxidation behavior of stainless steel 430 and 441 at 800 °C in single (air/air) and dual atmosphere (air/hydrogen) exposures, Int. J. Hydrogen Energy 33 (2008) 1392−1398, http://dx.doi.org/10.1016/j.ijhydene.2007.12.067.

[16] A.W. Bredvei Skilbred, R. Haugsrud, The effect of dual atmosphere conditions on the corrosion of Sandvik Sanergy HT, Int. J. Hydrogen Energy 37 (2012) 8095−8101, http://dx.doi.org/10.1016/j.ijhydene.2011.10.096.

[17] M.R. Ardigo, I. Popa, L. Combemale, S. Chevalier, F. Herbst, P. Girardon, Dual atmosphere study of the K41X stainless steel for interconnect application in high temperature water vapour electrolysis, Int. J. Hydrogen Energy (2015), http://dx.doi.org/10.1016/j.ijhydene.2015.01.116.

[18] H. Kurokawa, Oxidation behavior of Fe−16Cr alloy interconnect for SOFC under hydrogen potential gradient, Solid State Ionics 168 (2004) 13−21, http://dx.doi.org/10.1016/j.ssi.2004.02.008.

[19] D.J.L. Brett, A. Atkinson, N.P. Brandon, S.J. Skinner, Intermediate temperature solid oxide fuel cells, Chem. Soc. Rev. 37 (2008) 1568−1578, http://dx.doi.org/10.1039/b612060c.

[20] T. Jonsson, S. Canovic, F. Liu, H. Asteman, J.-E. Svensson, L.-G. Johansson, et al., Microstructural investigation of the effect of water vapour on the oxidation of alloy 353 MA in oxygen at 700 and 900 °C, Mater. High. Temp. 22 (2005) 231−243, http://dx.doi.org/10.3184/096034005782744461.

[21] J. Żurek, E. Wessel, L. Niewolak, F. Schmitz, T.-U. Kern, L. Singheiser, et al., Anomalous temperature dependence of oxidation kinetics during steam oxidation of ferritic steels in the temperature range 550−650 °C, Corros. Sci. 46 (2004) 2301−2317, http://dx.doi.org/10.1016/j.corsci.2004.01.010.

[22] D.J. Young, J. Zurek, L. Singheiser, W.J. Quadakkers, Temperature dependence of oxide scale formation on high-Cr ferritic steels in Ar−H2−H2O, Corros. Sci. 53 (2011) 2131−2141, http://dx.doi.org/10.1016/j.corsci.2011.02.031.

[23] L. Sánchez, M.P. Hierro, F.J. Pérez, Effect of chromium content on the oxidation behaviour of ferritic steels for applications in steam atmospheres at high temperatures, Oxid. Met. 71 (2009) 173−186, http://dx.doi.org/10.1007/s11085-008-9134-x.

[24] G.R. Holcomb, M. Ziomek-Moroz, S.D. Cramer, B.S. Covino, S.J. Bullard, Dual-environment effects on the oxidation of metallic interconnects, J. Mater. Eng. Perform. 15 (2006) 404−409, http://dx.doi.org/10.1361/105994906X117198.

[25] P. Gannon, R. Amendola, High-temperature, dual-atmosphere corrosion of solid-oxide fuel cell interconnects, JOM 64 (2012) 1470−1476, http://dx.doi.org/10.1007/s11837-012-0473-3.

[26] J. Froitzheim, H. Ravash, E. Larsson, L.G. Johansson, J.E. Svensson, Investigation of chromium volatilization from FeCr interconnects by a denuder technique, J. Electrochem. Soc. 157 (2010) B1295, http://dx.doi.org/10.1149/1.3462987.

[27] H. Falk-Windisch, J.E. Svensson, J. Froitzheim, The effect of temperature on chromium vaporization and oxide scale growth on interconnect steels for solid oxide fuel cells, J. Power Sources 287 (2015) 25−35, http://dx.doi.org/10.1016/j.jpowsour.2015.04.040.

[28] W.J. Quadakkers, J. Piron-Abellan, V. Shemet, L. Singheiser, Metallic interconnects for solid oxide fuel cells − a review, Mater. High. Temp. 20 (2003) 115−127, http://dx.doi.org/10.3184/096034003782749071.

[29] R. Amendola, P. Gannon, B. Ellingwood, K. Hoyt, P. Piccardo, P. Genocchio, Oxidation behavior of coated and preoxidized ferritic steel in single and dual atmosphere exposures at 800°C, Surf. Coatings Technol. 206 (2012) 2173−2180, http://dx.doi.org/10.1016/j.surfcoat.2011.09.054.

[30] F. Liu, J.E. Tang, T. Jonsson, S. Canovic, K. Segerdahl, J.-E. Svensson, et al., Microstructural investigation of protective and non-protective oxides on 11% chromium steel, Oxid. Met. 66 (2006) 295−319, http://dx.doi.org/10.1007/s11085-006-9035-9.

[31] T. Jonsson, B. Pujilaksono, H. Heidari, F. Liu, J.-E. Svensson, M. Halvarsson, et al., Oxidation of Fe−10Cr in O2 and in O2+H2O environment at 600°C: a microstructural investigation, Corros. Sci. 75 (2013) 326−336, http://dx.doi.org/10.1016/j.corsci.2013.06.016.

[32] B. Pujilaksono, T. Jonsson, H. Heidari, M. Halvarsson, J.-E. Svensson, L.-G. Johansson, Oxidation of binary FeCr alloys (Fe−2.25Cr, Fe−10Cr, Fe−18Cr and Fe−25Cr) in O2 and in O2 + H2O environment at 600 °C, Oxid. Met. 75 (2011) 183−207, http://dx.doi.org/10.1007/s11085-010-9229-z.

[33] H.E. Evans, A.T. Donaldson, T.C. Gilmour, Mechanisms of breakaway oxidation and application to a chromia-forming steel, Oxid. Met. 52 (1999) 379−402, http://dx.doi.org/10.1007/s11085-014-9237 (n.d.).

[34] N. Birks, G.H. Meier, F.S. Pettit, Mechanisms of oxidation, in: Introd. To High Temp. Oxid. Met, second ed., Cambridge University Press, New York, 2006, pp. 39−74.

[35] D. Whittle, G. Wood, D. Evans, D. Scully, Concentration profiles in the underlying alloy during the oxidation of iron-chromium alloys, Acta Metall. 15 (1967) 1747−1755, http://dx.doi.org/10.1016/0001-6160(67)90066-1.

[36] S.K. Yen, Critical hydrogen concentration for the brittle fracture of AISI 430 stainless steel, J. Electrochem. Soc. 143 (1996) 2736, http://dx.doi.org/10.1149/1.1837100.

[37] E. Essuman, G.H. Meier, J. Żurek, M. Hänsel, L. Singheiser, W.J. Quadakkers, Enhanced internal oxidation as trigger for breakaway oxidation of Fe−Cr alloys in gases containing water vapor, Scr. Mater 57 (2007) 845−848, http://dx.doi.org/10.1016/j.scriptamat.2007.06.058.

[38] E. Essuman, G.H. Meier, J. Żurek, M. Hänsel, W.J. Quadakkers, The effect of water vapor on selective oxidation of Fe−Cr alloys, Oxid. Met. 69 (2008) 143−162, http://dx.doi.org/10.1007/s11085-007-9090-x.

[39] J.E. Hammer, S.J. Laney, R.W. Jackson, K. Coyne, F.S. Pettit, G.H. Meier, The oxidation of ferritic stainless steels in simulated solid-oxide fuel-cell atmospheres, Oxid. Met. 67 (2007) 1−38, http://dx.doi.org/10.1007/s11085-006-9041-y.

[40] L. Niewolak, L. Garcia-Fresnillo, G.H. Meier, W.J. Quadakkers, Sigma-phase formation in high chromium ferritic steels at 650 °C, J. Alloys Compd. 638 (2015) 405−418, http://dx.doi.org/10.1016/j.jallcom.2015.03.076.

[41] L. Garcia-Fresnillo, V. Shemet, A. Chyrkin, L.G.J. de Haart, W.J. Quadakkers, Long-term behaviour of solid oxide fuel cell interconnect materials in contact with Ni-mesh during exposure in simulated anode gas at 700 and 800 °C, J. Power Sources 271 (2014) 213−222, http://dx.doi.org/10.1016/j.jpowsour.2014.07.189.

[42] L. Niewolak, E. Wessel, L. Singheiser, W.J. Quadakkers, Potential suitability of ferritic and austenitic steels as interconnect materials for solid oxide fuel cells operating at 600°C, J. Power Sources 195 (2010) 7600−7608, http://dx.doi.org/10.1016/j.jpowsour.2010.06.007.

[43] M. Stanislowski, J. Froitzheim, L. Niewolak, W.J. Quadakkers, K. Hilpert, T. Markus, et al., Reduction of chromium vaporization from SOFC interconnectors by highly effective coatings, J. Power Sources 164 (2007) 578−589, http://dx.doi.org/10.1016/j.jpowsour.2006.08.013.

[44] I. Belogolovsky, P.Y. Hou, C.P. Jacobson, S.J. Visco, Chromia scale adhesion on 430 stainless steel: effect of different surface treatments, J. Power Sources 182 (2008) 259−264, http://dx.doi.org/10.1016/j.jpowsour.2008.03.080.

[45] S. Canovic, J. Froitzheim, R. Sachitanand, M. Nikumaa, M. Halvarsson, L.-G. Johansson, et al., Oxidation of Co- and Ce-nanocoated FeCr steels: a microstructural investigation, Surf. Coatings Technol. 215 (2013) 62−74, http://dx.doi.org/10.1016/j.surfcoat.2012.08.096.

[46] M. Sattari, R. Sachitanand, J. Froitzheim, J.E. Svensson, T. Jonsson, The effect of Ce on the high temperature oxidation properties of a Fe−22%Cr steel: microstructural investigation and EELS analysis, Mater. High. Temp. 32 (2015) 118−122, http://dx.doi.org/10.1179/0960340914Z.00000000084.